Proceedings of the ASME 2023 18th International Mechanical Manufacturing Science and Engineering Conference
MSEC2023
June 12 - June 16, 2023, New Brunswick, NJ, USA

MSEC2023-104906

A FAST AND COST-EFFECTIVE IMAGING SYSTEM FOR FINE-SCALE TOOL CONDITION MONITORING IN ULTRASONIC METAL WELDING

Zhiqiao Dong[1], Qianmeng Chen[1], Kuan-Chieh Lu[1], Chenhui Shao[1,*]

[1]Department of Mechanical Science and Engineering, University of Illinois at Urbana-Champaign, Urbana, IL 61801, USA

ABSTRACT

In industrial-scale applications of ultrasonic metal welding (UMW), tool condition monitoring (TCM) is one of the most important maintenance tasks because tool health degrades quickly, and tool condition impacts the process physics and joint quality significantly. Moreover, tool replacement constitutes a notable portion of maintenance costs. In UMW, tool health degradation occurs mainly in the form of changes in tool surface geometry. Online TCM, which uses in-situ sensing data to indirectly classify tool conditions, has demonstrated to be effective; however, such indirect methods cannot provide a detailed characterization of tool surface profiles. On the other hand, direct measurements of tool surfaces require expensive and time-consuming high-resolution 3D metrology, which substantially increases the cost of quality and delays maintenance decision-making. To overcome these challenges, this paper develops a fast and cost-effective imaging system for fine-scale TCM in UMW. The imaging system mainly consists of a macro lens and a Raspberry Pi (RPI) high quality camera mounted over a linear rail driven by a stepper motor, and the full system is controlled through RPI GPIO (general-purpose input/output). The imaging system is used in conjunction with coaxial illumination, which enhances tool surface features, to capture a photo of a cast reproducing tool surface geometry. Then, image processing techniques are developed to characterize tool surface profiles and features. We demonstrate the effectiveness of the proposed TCM strategy using tools in three distinct conditions. Results show that the TCM imaging system can effectively reconstruct critical fine-scale geometric features of tools, thus enabling more responsive, interpretable, and reliable TCM for UMW.

Keywords: tool condition monitoring, surface metrology, ultrasonic metal welding, machine vision, computer vision, maintenance, quality control

*Corresponding author: chshao@illinois.edu

1. INTRODUCTION

Ultrasonic metal welding (UMW) is an advantageous solid-state joining technique for thin metal materials, and has wide industrial utility [1, 2], such as lithium-ion battery assembly [3–6], automotive body construction [7–9], and electronic packaging [10, 11]. UMW uses ultrasonic vibration to generate oscillating shears between metal layers clamped under pressure [12–14]. Fig. 1 illustrates a typical UMW system. In an UMW process, workpieces are placed between and clamped by the two tool components, i.e., horn and anvil. The anvil stays stationary while the horn vibrates at a frequency of around 20 kHz. The surfaces of horn and anvil consist of repetitive pyramid-shaped knurls as shown in Fig. 2. In production, the knurl patterns change quickly because of the strong friction and relative movements [14, 15] that exist at interfaces between welding tools and workpieces.

Since UMW tool conditions significantly impact the process physics and further the joint quality, tools must be replaced in time before they wear out to guarantee satisfactory product quality [15, 17]. Moreover, tool replacement leads to significant production costs including machine down time and expenses for fabricating, reworking, or refurbishing the replaced tools, which is reported to constitute a notable part of maintenance costs [15, 17]. Without the ability to accurately monitor the tool wear, a conservative tool replacement strategy is generally adopted in industry. For example, the tools are replaced once a certain number of welds has been produced. This empirical strategy is straightforward to implement, but it does not account for machine-to-machine or tool-to-tool variability. Thus, it may waste useful tool lives and cannot detect abnormally fast tool wear, e.g., due to tool installation faults. As a result, a tool condition monitoring (TCM) system is critically needed to reduce tool replacement costs while ensuring joint quality.

TCM has been an important topic in manufacturing and tremendous research has been conducted. While the majority of the TCM literature has concentrated on machining processes [18–21], limited studies have been conducted for UMW. It is more challenging to monitor tools for UMW than other manufacturing

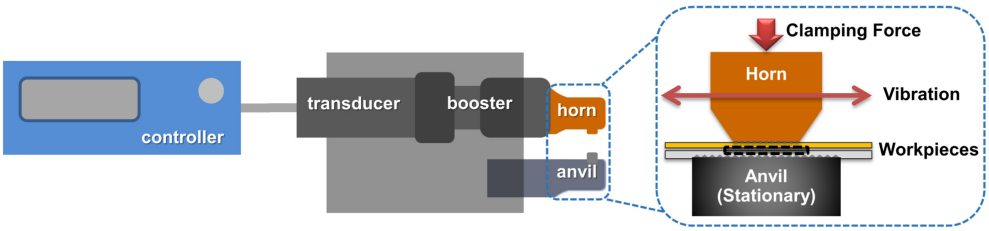

FIGURE 1: CONFIGURATION OF A TYPICAL UMW SYSTEM [16].

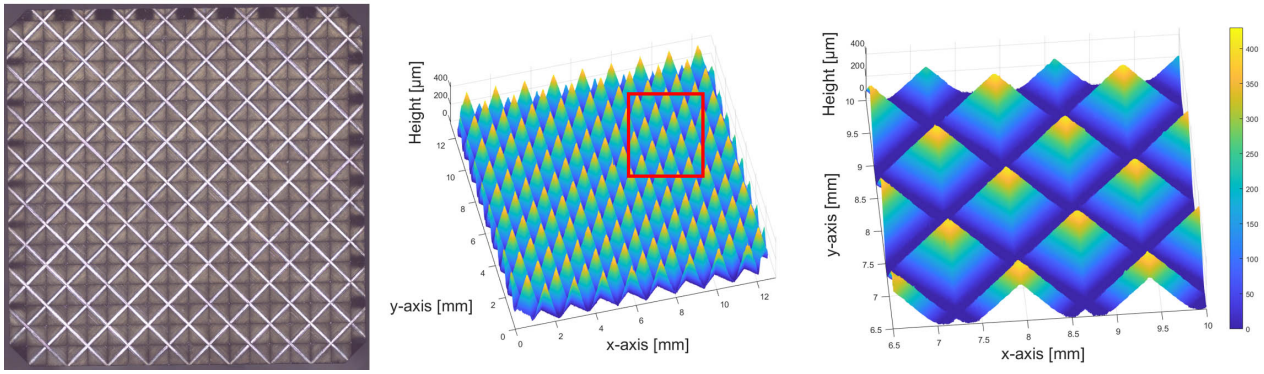

(a) A new anvil surface.

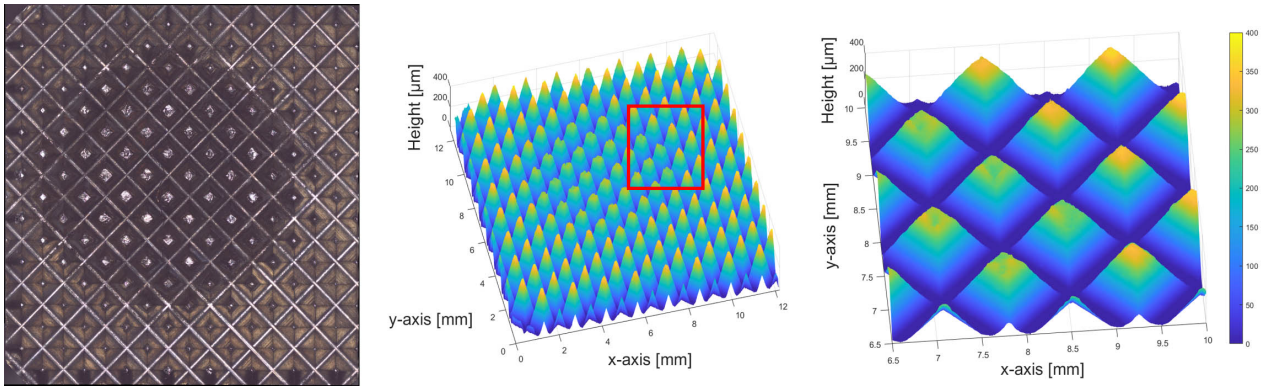

(b) A half-worn anvil surface.

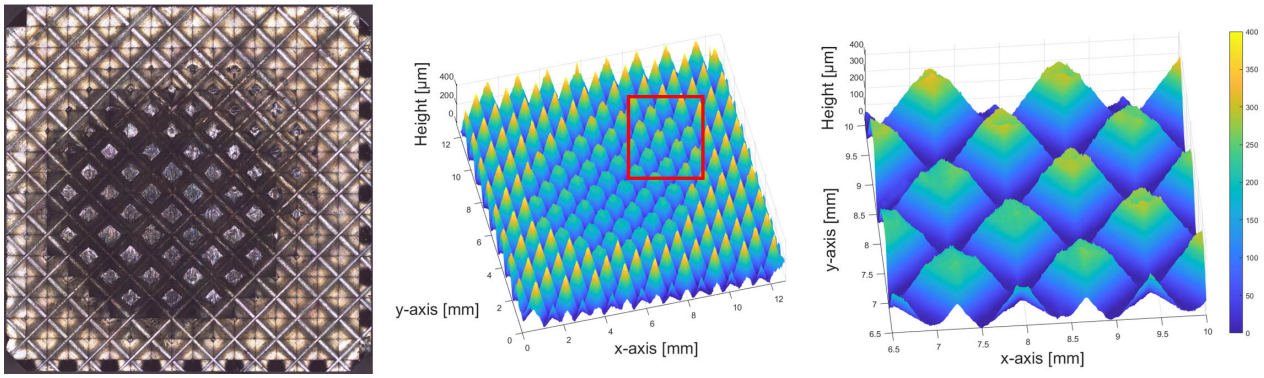

(c) A completely worn anvil surface.

FIGURE 2: ANVIL SURFACES OF DIFFERENT WEAR STAGES. IN EACH ROW: (LEFT) OPTICAL PHOTO, (MIDDLE) HIGH-RESOLUTION 3D MEASUREMENT, AND (RIGHT) A ZOOM-IN VIEW OF 3D MEASUREMENT.

processes, mainly because: (1) the geometry of UMW tools is much more complicated [17, 22, 23], and (2) the UMW process runs at a high oscillation frequency (typically about 20 kHz) with short welding cycles (often below 1 s), and its mechanism has not been thoroughly understood [15, 17].

In general, TCM strategies can be categorized into direct and indirect methods, depending on whether the tool geometry is directly examined. Indirect TCM methods, e.g., [15, 24–28], use online sensing data to infer on and classify tool conditions. Shao et al. [15] adopted the dominant frequency of the sound signal from microphone as the major feature, and correlated it with the weld count that serves as a tool wear indicator. Shi et al. [26] proposed a method to monitor the anvil tool installation condition using acceleration signals. A sensor fusion-based online TCM system was established in [25] using features generated from power, displacement, sound, and acoustic emission signals. The feature generation procedure and classifiers were further improved in [27] with close-to-perfect classification accuracy achieved.

While indirect methods are capable of online monitoring and demonstrated to be effective in classification, they have some limitations. Indirect methods require in-situ sensors and a data acquisition system as prerequisites, which pose substantial costs. Moreover, indirect methods cannot provide a detailed characterization of tool surface profiles. In UMW, tool health degradation occurs mainly in the form of changes in tool surface geometry, which progresses continuously and can display various, complicated patterns [15, 17]. Thus, it is not sufficient to simply classify a tool into good or worn conditions. In addition, because no existing models can effectively correlate peripheral sensor signals with the UMW tool surface profiles, and the process variation is usually significant, the interpretability of indirect methods can be insufficient for high-precision TCM and other advanced decision-making tasks including predictive maintenance and process control.

By measuring the tool surface profiles, direct TCM strategies overcome the limitations of indirect methods. For UMW, such TCM methods are reported in [15, 17, 29]. The UMW tool wear progression was first characterized in [15], which categorized tool wear into four different stages and described their surface geometry with 3D measurements. To avoid tedious disassembly and reassembly of tools, an impression method was proposed in [17] to produce a metal weld coupon that reproduces the tool surface shape for inspection, and features were then generated using cross-sectional surface profiles for TCM. A high-order decomposition method was presented in [29] to further improve the feature extraction and monitoring procedure. However, all of these direct methods depend on high-resolution 3D measurements of tool surfaces or their surrogates. The expensive and time-consuming measurement procedure substantially increases the cost of quality and delays maintenance decision-making [30].

Recently, some studies developed interpolation methods based on spatial modeling [22] and multi-task learning [23] to improve the measurement efficiency. While these methods can reduce the requirement on high-resolution metrology, they still require disassembly and reassembly of tools. Moreover, a relatively dense measurement of the tool surfaces is required to ensure satisfactory interpolation accuracy.

Compared with 3D measurements, 2D photos of high-resolution can be obtained in a much faster and cheaper fashion using cameras. There have been numerous studies about TCM with images for machining processes (e.g., [20, 21, 31–34]). Yet, none of the existing TCM methods for UMW, except human visual inspection, adopt 2D images. Since evident tool wear can be easily identified by human eyes through a magnifier, in principle, monitoring of UMW tools is also possible using machine vision, despite the loss of 3D information. Thus, in this paper, we develop an imaging system and image processing techniques to enable fast, cost-effective, and fine-scale TCM in UMW. The imaging system is used in conjunction with coaxial illumination, which enhances tool surface features, to capture a photo of a thermoplastic resin cast reproducing tool surface geometry.

The rest of this paper is organized as follows. Section 2 proposes and describes the worn area size as an essential index of UMW tool degradation. Section 3 presents an improved impression method for tool geometry measurement and demonstrate the benefit of coaxial illumination. Section 4 introduces a cost-effective implementation of an imaging system for TCM in UMW. Image processing techniques are developed in Section 5 to characterize worn area and extract features for tool condition classification. Finally, Section 6 concludes the paper and suggests future research directions.

2. WORN AREA SIZE AS A TOOL WEAR INDEX

This section first demonstrates that the degree of tool wear can be adequately characterized by the worn area, i.e., where material removal takes place. Then, a heuristic description for worn area is provided, which is readily translatable into corresponding features in 2D images.

Optical photos and high-resolution 3D measurements (all captured with a Keyence VK-X1000 confocal laser scanning microscope) of three sample surfaces are shown in Fig. 2, which correspond to anvils that are empirically categorized as brand-new, half-worn, and completely worn. We refer to these anvils as surface 1, 2, and 3, respectively. Knurls are small-scale. In a new condition, the knurl pyramid is 0.44 mm in height and 1.44 mm in diagonal. Fig. 3 shows several cross-sectional profiles from knurl tops in different conditions. According to measurements, the three knurls undergo different levels of material removal. The typical progression mode was reported and characterized in [15].

The 3D measurements reveal an obvious overall trend: knurl height decreases and the top becomes flat as tool wear progresses. In addition, the area where material removal occurs can be clearly recognized from both 3D measurements and photos in Fig. 2, and worn areas expand monotonically as more material is abraded from the surface. The latter observation suggests the use of worn area size, which can be identified from optical images without 3D information, as an informative index of tool wear.

Worn area size has several additional advantages over other characterizations:

(1) It is a well-defined physical quantity depending only on the tool surface. Unlike the crude classification of tools into discrete stages, it does not depend on human judgment. Nor does it rely on machine operation conditions, like the weld

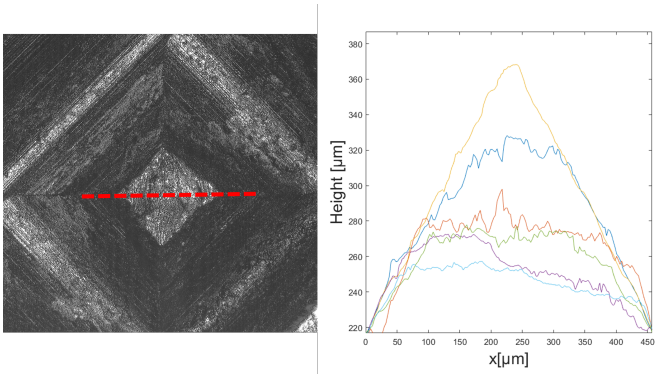

FIGURE 3: TYPICAL CROSS-SECTIONAL PROFILES OF ANVIL KNURL TOPS IN DIFFERENT CONDITIONS.

counts.

(2) It can be defined for individual knurls to describe the spatial distribution of surface degradation, enabling more detailed characterization of tool wear patterns.

(3) Compared with features extracted from 1D cross-sectional profiles in [17], computing the size of a two-dimensional area involves more measurement points, which indicates a better utilization of data and improved robustness to measurement noise.

While the worn area is physically well-defined and recognizable to human, it remains challenging to automatically identify worn area with an algorithm. We may use the following heuristic characterizations: worn area can be approximately described as areas (1) around knurl centers, (2) with a notable portion of which being flat on average at a larger scale (~0.5 mm), and (3) whose surface is rough with notable variation at a smaller scale (~50 µm), as shown by the 3D measurements in Fig. 2 and sectional profiles in Fig. 3. Note that, the latter two conditions intuitively result in an interesting property: local minima and maxima are densely distributed in worn areas. At the same time, extrema are expected to be sparser on the four faces of knurls, whose slope outweighs variation at smaller scales. Consequently, worn area can be distinguished from unworn region surrounded according to extrema density, which will be converted into discernible features in images with the help of illumination (Section 3.2).

3. ACQUISITION OF TOOL SURFACE PROFILES AND FEATURES

Surface geometry of UMW tools provides essential tool condition information. It is necessary to avoid tool disassembly for both measurement efficiency and production cost reduction. Section 3.1 describes an impression method for surface measurement, improving the existing work [17]. Then, Section 3.2 illustrates how the worn area can be enhanced in images via coaxial illumination for easier identification.

3.1 Impression Method

Previously, an impression method was proposed in [17] to reduce the production down-time. Rather than measuring the tool directly, it makes an impression on a metal weld coupon. Fig. 4 shows an example. Then, the tool surface height corresponds to

FIGURE 4: A METAL COUPON PRODUCED BY THE IMPRESSION METHOD IN [17].

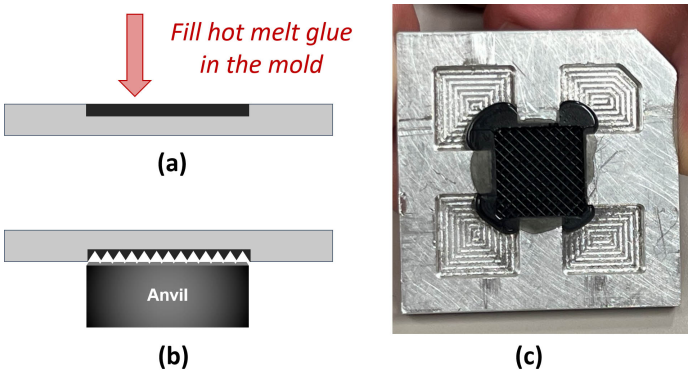

FIGURE 5: CAST PRODUCTION PROCEDURE.

the inverse of coupon deformation depth, which is measured as a surrogate of the tool surface using a 3D measurement system.

Although a good agreement was demonstrated between the tool surface and its weld coupon, there are still some issues with the existing impression method. First, the metal coupon may not fully reproduce the tool geometry. In a typical aluminum coupon shown in Fig. 4, only the central area of the tool is well represented by the impression. Second, material and parameter combinations have to be tested for good indentation, and the optimal parameters vary with time as the tool gradually wears out. Third, it generally requires a high welding energy, often beyond the range of normal operation, to make a deep and full impression, which is neither energy efficient nor convenient. Further, in such cases, materials like aluminum may adhere to the tool and stain the surface. Once it happens, the tool has to be disassembled and cleaned in strong bases, causing extra machine down-time. Welding with excessively high energy also increases the risk of tool damage.

Noticing that these issues arise essentially due to insufficient plasticity of the metal coupon, we propose to make casts with more plastic materials, e.g., resins. Fig. 5 illustrates the procedure for producing casts. We use hot melt glue, which is a cheap and easily accessible type of thermoplastic resin, as the casting material in this research. To produce the cast, we first fill hot melt glue into a mold (Fig. 5a), which is a piece of aluminum with a shallow groove on the top that matches the contour of the tool (UMW anvil in this case). Then, the mold is aligned with the tool and then pressed to let the knurls dent into the molten glue (Fig. 5b). The mold can be removed from the tool after the glue

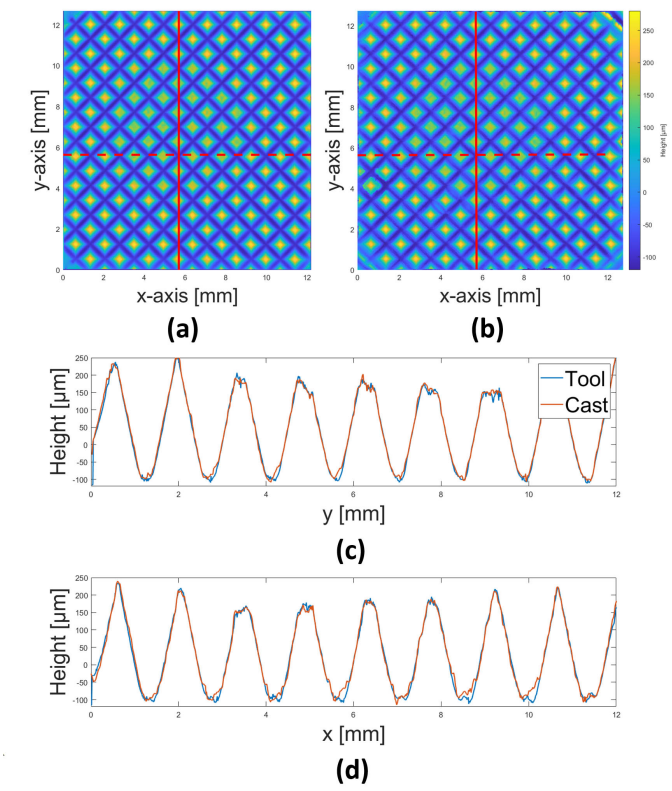

FIGURE 6: COMPARISON OF ANVIL 2 AND ITS CAST. (A) 3D MEASUREMENT OF THE ORIGINAL SURFACE. (B) 3D MEASUREMENT OF THE CAST. (C) A CROSS-SECTIONAL PROFILE IN THE VERTICAL DIRECTION INDICATED BY THE SOLID RED LINE IN (A) AND (B). (D) A CROSS-SECTIONAL PROFILE IN THE HORIZONTAL DIRECTION INDICATED BY THE DASHED RED LINE IN (A) AND (B).

has cooled down, and a cast shown in Fig. 5c is produced.

To validate this method, casts of anvil surfaces 1, 2, and 3 are created and measured for comparison. Good agreement is achieved between the original tools and inverse casts. For example, Fig. 6a and 6b display 3D measurements of anvil 2 and its cast, and two typical cross-sectional profiles marked with red lines are compared in Fig. 6c and 6d. It is worth noting that small-scale geometric patterns, e.g., on the top of knurls, are captured well, suggesting a good potential for fine-scale characterization and monitoring.

3.2 Feature Enhancement via Coaxial Illumination

Since the cast is expected to faithfully reproduce the tool surface, the heuristic properties of worn area proposed in Section 2 should remain valid for corresponding regions over the cast surface. Thus, we may distinguish the worn area in the image by enhancing locations of extrema, where the surface has normal direction perpendicular to the horizontal plane. When the camera views from the top, such points can be highlighted over specular surfaces with coaxial lighting that is roughly collimated, as depicted in Fig. 7.

Coaxial illumination refers to the case where front light hits the object surface perpendicular to the object plane, as illustrated

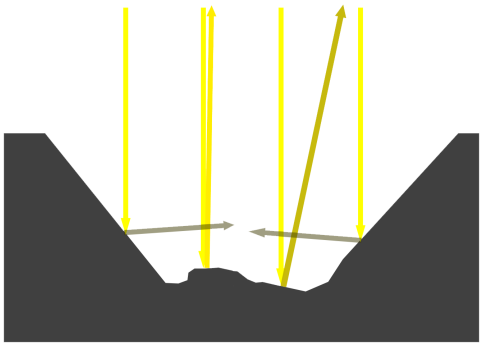

FIGURE 7: LOCAL EXTREMA ARE HIGHLIGHTED AND SLOPED SURFACES ARE DIMINISHED GIVEN COLLIMATED COAXIAL LIGHTING.

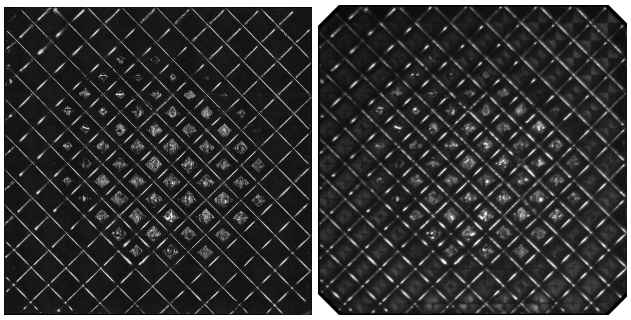

(a) Laser intensity image **(b) Our alternative.**

FIGURE 8: IMAGES OF A CAST FOR SURFACE 3 UNDER (A) COMMERCIAL COLLIMATED COAXIAL LASER AND (B) APPROXIMATELY COAXIAL ILLUMINATION.

by Fig. 9. Approximate collimation requires rays to be parallel to the optical axis within a certain degree. Over a specular surface, points with roughly perpendicular normal will be highlighted in images under such light according to the law of reflection, while slopes will be darker. Consequently, the worn area is bright in images, filled with shiny spots corresponding to extrema locations and darker transition pixels in between; and intact regions will appear mostly dark. The contrast can be further enhanced with image derivatives in later processing. Fig. 8 compares the images of a cast for surface 3 obtained using a Keyence VK-X1000 confocal laser scanning microscope and our own system. Fig. 8a can be regarded as a photo taken with precisely collimated coaxial illumination. The image presents highlights and shadows as expected. A photo captured with our own system (Fig. 8b) shows comparable patterns compared with Fig. 8a, demonstrating the effectiveness of the system.

The choice of the casting material can be further explained from an imaging perspective. Hot melt glue has fine and uniform texture that makes cast surfaces specular. Furthermore, the glue is chosen to be black, in order to suppress unhelpful body reflection.

4. IMPLEMENTATION OF A COST-EFFECTIVE IMAGING SYSTEM

A cost-effective imaging system is developed to implement the proposed TCM strategy. The design and implementation

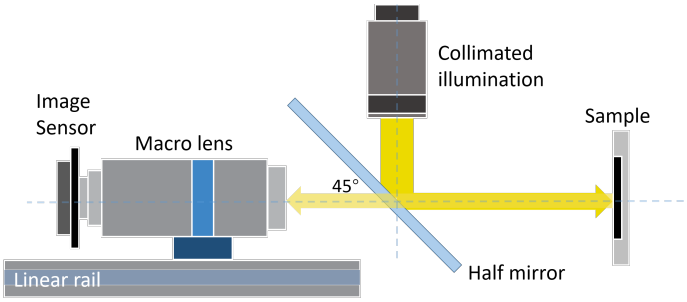

FIGURE 9: A SCHEMATIC DIAGRAM OF THE IMAGING SYSTEM.

avoid using expensive industrial-grade components by adopting economic consumer-grade alternatives, in order to make it more accessible to manufacturers. A schematic of the system is shown in Fig. 9.

The imaging system mainly consists of a macro lens and a Raspberry Pi (RPI) high quality camera mounted over a linear rail driven by a stepper motor, and the full system is controlled through RPI GPIO (general-purpose input/output). Instead of purchasing a professional coaxial light, we use a pinspot light as a roughly collimated light source together with a teleprompter glass to achieve coaxial illumination. Major components of the system are listed in Table 1, which cost less than $500 in total. Components are assembled on a frame of aluminum extrusions with screws and some 3D printed connectors. A photo for an assembled system is shown in Fig. 10.

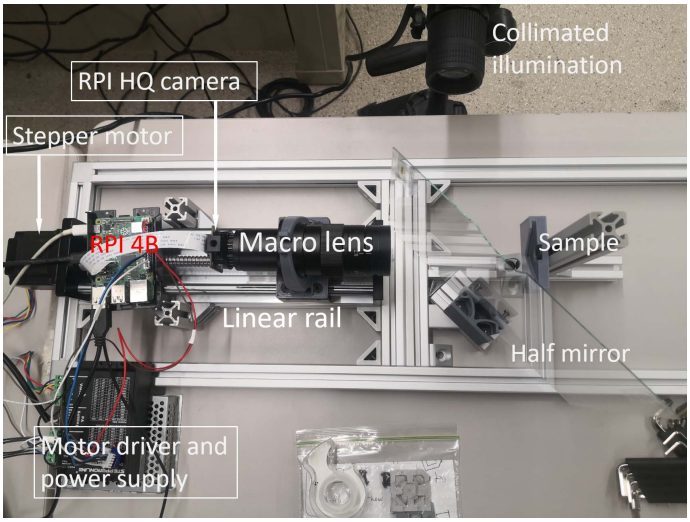

FIGURE 10: PHOTO OF THE ASSEMBLED IMAGING SYSTEM.

5. FEATURE EXTRACTION FROM IMAGES AND TOOL CONDITION CLASSIFICATION

In Section 5.1, we sketch the procedure for processing the images and explain how it is developed. Then, the size of identified area is used together with image brightness for effective and interpretable classification in Section 5.2. Fig. 11 summarizes the complete TCM procedure with cast images.

TABLE 1: LIST OF COMPONENTS IN THE IMAGING SYSTEM.

Component	Model
Image sensor	RPI HQ camera
Lens	Unbranded, from a microscope for electronics repair
Coaxial illumination	A pinspot light A teleprompter glass
Motorized focus control	An inexpensive linear rail driven by a stepper motor RPI 4B Stepper motor driver DC power supply for stepper motor

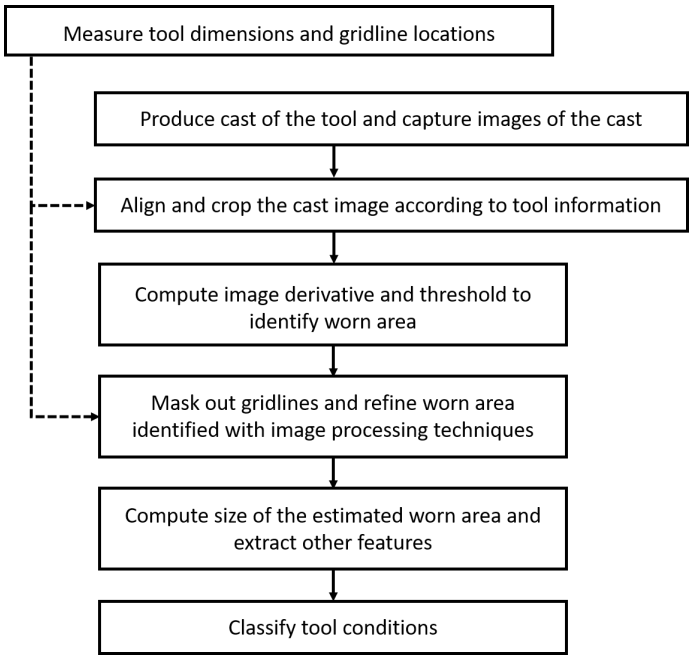

FIGURE 11: A FLOWCHART FOR TCM OF UMW WITH CAST IMAGES.

5.1 Worn Area Identification from Cast Images

With the imaging system, we are able to obtain photos of the casts, e.g., Fig. 8b for surface 3 or Fig. 12d for surface 2. Because our low-cost system does not provide ideally even and collimated illumination, it does not work very well to threshold directly on the photo. Instead, we enhance the contrast between worn area by computing the image derivative. Compared with the raw image (e.g., Fig. 12d), thresholding on the image Laplacian (Fig. 12e) can yield a better segmentation result.

The entire processing procedure is developed to complement the thresholding operation on the image derivative. To make comparison between different photos sensible, the impression area has to be correctly separated from the background. Also, thresholding highlights the gridlines, which are valleys between knurls. Such interference has to be masked before counting pixels for worn area size estimation. Morphological reconstruction is applied to remove the gridlines once their locations are identified. Prior knowledge about the tool dimensions can be incorporated to make the process more robust. The complete procedure for

processing a cast image is summarized as follows:

(1) Measure dimensions and gridline locations (Fig. 12c) of the same tool that produces the cast. Such information can be obtained from an image of the tool, which can be captured before tool installation in practice.

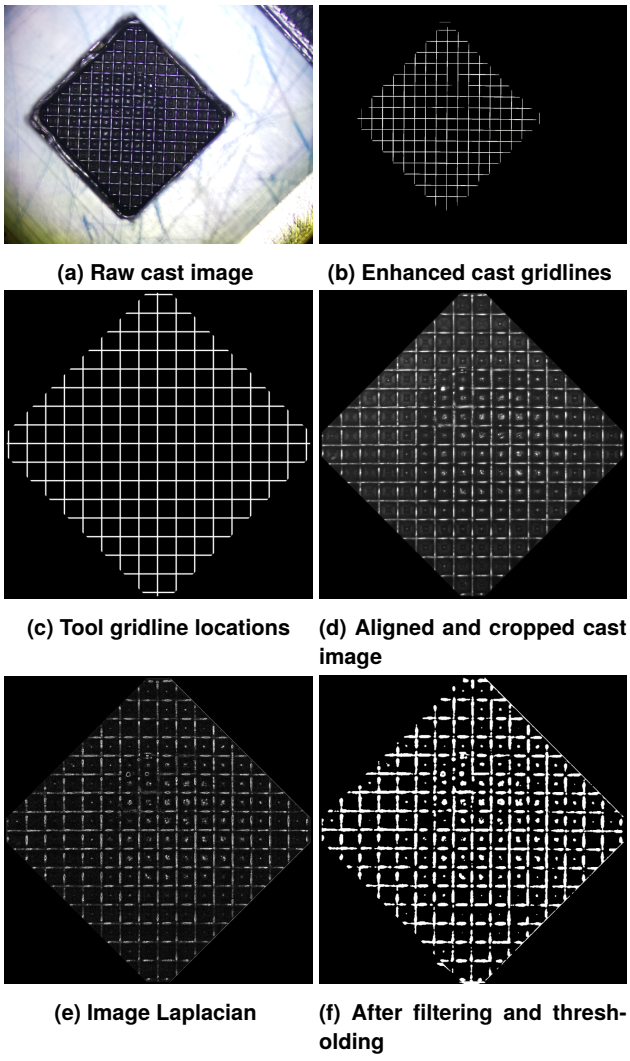

(a) Raw cast image (b) Enhanced cast gridlines

(c) Tool gridline locations (d) Aligned and cropped cast image

(e) Image Laplacian (f) After filtering and thresholding

FIGURE 12: IMAGE PROCESSING PROCEDURE FOR WORN AREA IDENTIFICATION WITH CAST IMAGES. CAST 1 OF SURFACE 2 IS USED FOR ILLUSTRATION.

(2) Identify the impression area and gridlines (Fig. 12b) roughly on the raw cast image (Fig. 12a), which are then matched with the corresponding tool information to accurately align and crop the image, leaving only the impressed area unmasked (Fig. 12d).

(3) Compute image Laplacian (Fig. 12e), smooth and apply an adaptive thresholding (Fig. 12f), such that worn areas together with gridlines are marked bright. With the tool information (Fig. 12c) from (1), mask out the gridlines.

(4) Connect the identified worn area and remove scattered misdetections with an order-statistic filter, and then refine the result with a close and an open morphological operation, in order to connect identified fragments and trim small marks that are possibly misdetected. The final result is marked in Fig. 13c.

Fig. 13 displays the segmentation results of cast images of surfaces 1, 2, and 3. The worn area identified is consistent with visual inspection, and increases as tool wear progresses.

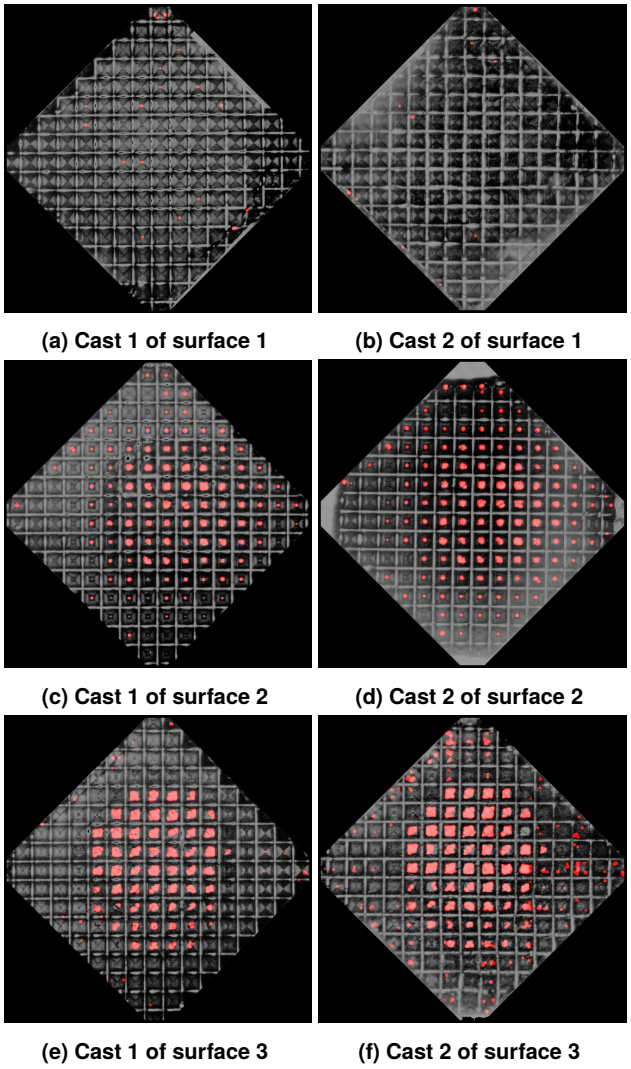

(a) Cast 1 of surface 1 (b) Cast 2 of surface 1

(c) Cast 1 of surface 2 (d) Cast 2 of surface 2

(e) Cast 1 of surface 3 (f) Cast 2 of surface 3

FIGURE 13: IDENTIFIED WORN AREA FOR IMAGES OF DIFFERENT CASTS.

5.2 Tool Condition Classification

After worn areas are identified in cast images, the number of marked pixels can be used to estimate the area size. There are always errors in the segmentation result following the previous procedure. Some worn locations are not correctly marked, while many intact spots are mistakenly labeled because of cast imperfection or uneven illumination, etc. Besides, variations exist in segmentation results of cast photos for the same tool surface, because of different casts and camera/sample settings.

Despite these variations, significant difference is still observed between the identified area sizes of different tool conditions, comparing different rows of Fig. 13. In this research, three casts are produced and imaged for each surface. Some of the casts (three for surface 2 and one for surfaces 1 and 3 each) are imaged

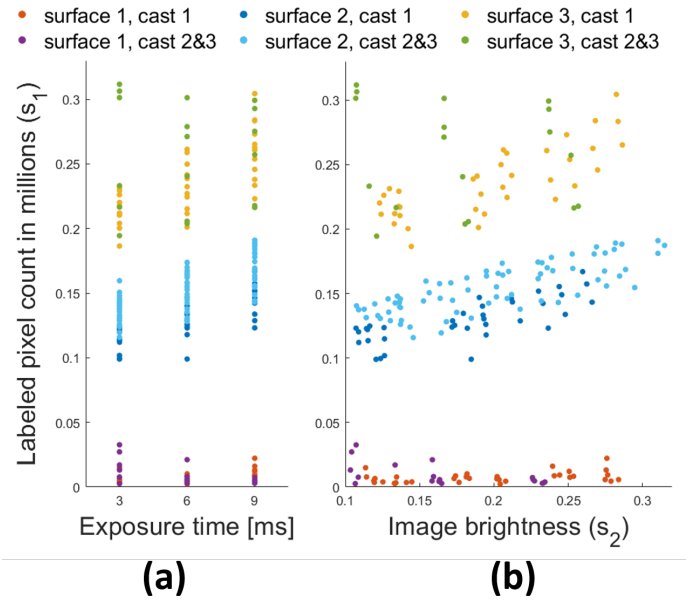

FIGURE 15: NUMBER OF LABELED PIXELS VERSUS IMAGE STATISTICS, (A) EXPOSURE TIME AND (B) IMAGE BRIGHTNESS.

at two different mounting locations. For the third cast of surface 2, the light is adjusted to hit the sample in three slightly different angles. Every time the cast and light are fixed, nine photos are taken for all combinations of 3/6/9 ms exposure time and three slightly different objective distances in focus.

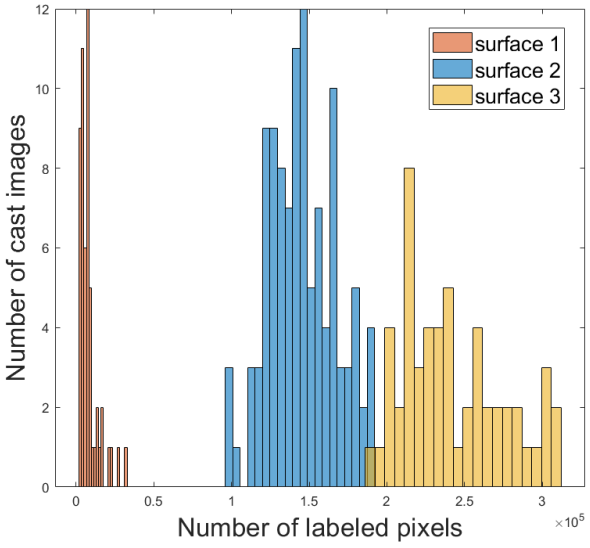

FIGURE 14: HISTOGRAMS FOR LABELED PIXEL COUNT IN CAST IMAGES OF THREE TOOL SURFACES.

The segmentation procedure in Section 5.1 is carried out for each photo, and the pixel counts for different surfaces are summarized in Fig. 14. Although it shows good separability, there are still some overlaps for half-worn and completely worn

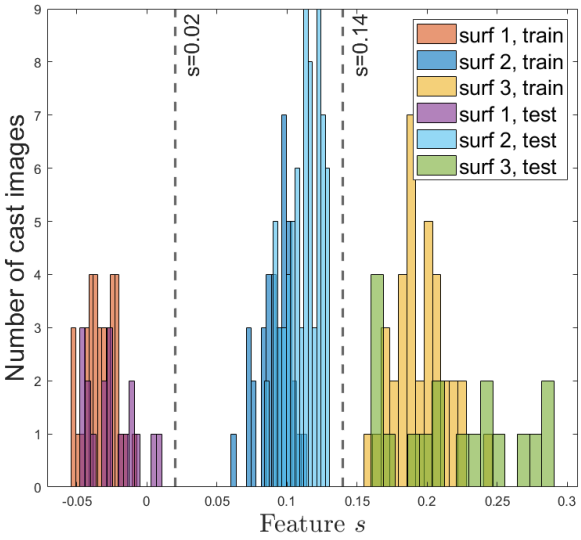

FIGURE 16: HISTOGRAMS FOR THE FEATURE s OF CAST IMAGES.

tools. However, perfect separability can be achieved, once we fix the exposure time (Fig. 15a) or take the photo brightness into consideration (Fig. 15b). Consequently, the worn pixel count estimated following the described segmentation procedure from cast images should serve well as an indicator of tool wear once corrected with statistics characterizing photo brightness. Note that images are not adjusted for uniform brightness before segmentation using conventional grayscale transforms such as histogram equalization, because such operation may impede the thresholding procedure.

The classification task is straightforward due to the clear separability. To demonstrate the effectiveness, we use the pixel count in millions (s_2) and image brightness (s_1) as the features, and identify an optimal direction of separation with multiclass linear discrimination analysis (LDA) [35, 36]. As an example, the first cast of the three surfaces are used to generate features for the training set, and the remaining casts for the test set. Then, for best separability the LDA procedure suggests using $s = s_2 - 0.21 s_1$, which has a clear physical explanation as an estimated worn area size after adjustment according to exposure conditions. The histogram using the feature s is plotted in Fig. 16. It is obvious that naive thresholding (e.g., with $s = 0.02$ and $s = 0.14$) would already be sufficient for 100% accuracy. The classification robustness can be further improved by constructing separation hyperplanes pairwisely without requiring them to be parallel.

6. CONCLUSION AND FUTURE WORK

Tool wear identification and monitoring for UMW using images are investigated in this paper. By comparing 3D measurements and optical images of tool surfaces in different conditions, worn area and its size are demonstrated to be critical fine-scale geometric features for tool wear characterization and monitoring. In addition, the worn area can be identified from 2D images of either the tool surface or its cast, especially when produced with black thermoplastic resin and illuminated using coaxial light.

The cast reproduces the tool surface geometry accurately, and is measured as a substitution to minimize production interruption. A cost-effective imaging system is designed and implemented to capture cast photos. We develop an image processing procedure to identify worn area from cast photos. It is shown that the worn area size can be adequately estimated for a tool surface from its cast photos. Tool condition classification with the proposed features becomes more straightforward and interpretable.

The developed imaging system eliminates the need of slow and expensive high-resolution 3D measurement system and enables images from conventional cameras to identify fine-scale wear areas on UMW tool surfaces, allowing faster data acquisition at lower cost for more responsive and accessible TCM. Performance of the current monitoring system could be further improved with more accurate image segmentation algorithm. Besides, correlation between images and 3D measurements is worth exploring for further utilization of image information. Finally, tool wear can be characterized at knurl level. The spatial pattern of knurl degradation may be useful for various advanced monitoring and diagnosis tasks in UMW.

Additionally, the proposed framework for TCM may be generalized to other surface abrasion monitoring tasks, when the degradation can be well-characterized by the expansion of the worn area, which has discernible features compared with intact area in optical photos. In such applications, the following guidelines may be considered to adapt the procedure. First, the impression method is helpful when it is inconvenient to image the surface itself. Apart from this, uniformity of the casting material improves the consistency of imaging quality, especially when the color information is complicated, irrelevant or ambiguous. Second, coaxial and collimated illumination highlights extrema over specular surfaces, while the imaging and illumination configuration should be re-designed when the worn area cannot be distinguished by extrema-related features. After obtaining informative photos, application-specific procedures can be established for segmentation and other high-level tasks. Third, irrelevant information or interference can be masked out by incorporating process knowledge (such as tool gridline locations in this work), or computing the difference between images after alignment and adjustments.

7. ACKNOWLEDGMENT

This research has been supported by the National Science Foundation under Grant No. 1944345. The experiments were carried out in part in the Materials Research Laboratory Central Research Facilities, University of Illinois.

REFERENCES

[1] Kumar, S, Wu, CS, Padhy, GK and Ding, W. "Application of ultrasonic vibrations in welding and metal processing: A status review." *Journal of manufacturing processes* Vol. 26 (2017): pp. 295–322.

[2] Cheng, X. M., Yang, K., Wang, J., Xiao, W. T. and Huang, S. S. "Ultrasonic system and ultrasonic metal welding performance: A status review." *Journal of Manufacturing Processes* Vol. 84 (2022): pp. 1196–1216.

[3] Kim, Tae H, Yum, J, Hu, S Jack, Spicer, JP and Abell, Jeffrey A. "Process robustness of single lap ultrasonic welding of thin, dissimilar materials." *CIRP annals* Vol. 60 No. 1 (2011): pp. 17–20.

[4] Lee, S Shawn, Kim, Tae Hyung, Hu, S Jack, Cai, Wayne W, Abell, Jeffrey A and Li, Jingjing. "Characterization of joint quality in ultrasonic welding of battery tabs." *Journal of Manufacturing Science and Engineering* Vol. 135 No. 2 (2013).

[5] Kang, Bongsu, Cai, Wayne and Tan, Chin-An. "Dynamic response of battery tabs under ultrasonic welding." *Journal of Manufacturing Science and Engineering* Vol. 135 No. 5 (2013).

[6] Nong, Lihang, Shao, Chenhui, Kim, Tae Hyung and Hu, S Jack. "Improving process robustness in ultrasonic metal welding of lithium-ion batteries." *Journal of Manufacturing Systems* Vol. 48 (2018): pp. 45–54.

[7] Ni, ZL and Ye, FX. "Ultrasonic spot welding of aluminum alloys: A review." *Journal of Manufacturing Processes* Vol. 35 (2018): pp. 580–594.

[8] Siddiq, Amir and Ghassemieh, Elaheh. "Thermomechanical analyses of ultrasonic welding process using thermal and acoustic softening effects." *Mechanics of Materials* Vol. 40 No. 12 (2008): pp. 982–1000.

[9] Zhang, CY, Chen, DL and Luo, AA. "Joining 5754 automotive aluminum alloy 2-mm-thick sheets using ultrasonic spot welding." *Weld. J* Vol. 93 No. 4 (2014): pp. 131–138.

[10] Kim, Jongbaeg, Jeong, Bongwon, Chiao, Mu and Lin, Liwei. "Ultrasonic bonding for MEMS sealing and packaging." *IEEE Transactions on Advanced Packaging* Vol. 32 No. 2 (2009): pp. 461–467.

[11] Vianco, Paul T. "A Review of Interface Microstructures in Electronic Packaging Applications: Brazing and Welding Technologies." *JOM* Vol. 74 No. 9 (2022): pp. 3557–3577.

[12] Lee, Shawn S., Shao, Chenhui, Kim, Tae Hyung, Hu, S. Jack, Kannatey-Asibu, Elijah, Cai, Wayne W., Spicer, J. Patrick and Abell, Jeffrey A. "Characterization of Ultrasonic Metal Welding by Correlating Online Sensor Signals With Weld Attributes." *Journal of Manufacturing Science and Engineering* Vol. 136 No. 5 (2014).

[13] Lee, Shawn S., Kim, Tae Hyung, Hu, S. Jack, Cai, Wayne W., Abell, Jeffrey A. and Li, Jingjing. "Characterization of Joint Quality in Ultrasonic Welding of Battery Tabs." *Journal of Manufacturing Science and Engineering* Vol. 135 No. 2 (2013).

[14] Lee, Shawn S., Kim, Tae Hyung, Hu, S. Jack, Cai, Wayne W. and Abell, Jeffrey A. "Analysis of Weld Formation in Multilayer Ultrasonic Metal Welding Using High-Speed Images." *Journal of Manufacturing Science and Engineering* Vol. 137 No. 3 (2015).

[15] Shao, Chenhui, Guo, Weihong, Kim, Tae H, Jin, Jionghua Judy, Hu, S Jack, Spicer, J Patrick and Abell, Jeffrey A. "Characterization and monitoring of tool wear in ultrasonic metal welding." *9th International Workshop on Microfactories*: pp. 161–169. 2014.

[16] Meng, Yuquan, Rajagopal, Manjunath, Kuntumalla, Gowtham, Toro, Ricardo, Zhao, Hanyang, Chang, Ho Chan,

Sundar, Sreenath, Salapaka, Srinivasa, Miljkovic, Nenad, Ferreira, Placid, Sinha, Sanjiv and Shao, Chenhui. "Multi-objective optimization of peel and shear strengths in ultrasonic metal welding using machine learning-based response surface methodology." *Mathematical Biosciences and Engineering* Vol. 17 No. 6 (2020).

[17] Shao, Chenhui, Hyung Kim, Tae, Jack Hu, S., (Judy) Jin, Jionghua, Abell, Jeffrey A. and Patrick Spicer, J. "Tool Wear Monitoring for Ultrasonic Metal Welding of Lithium-Ion Batteries." *Journal of Manufacturing Science and Engineering* Vol. 138 No. 5 (2016).

[18] Mohanraj, T, Shankar, S, Rajasekar, R, Sakthivel, NR and Pramanik, Alokesh. "Tool condition monitoring techniques in milling process—a review." *Journal of Materials Research and Technology* Vol. 9 No. 1 (2020): pp. 1032–1042.

[19] Serin, Gokberk, Sener, Batihan, Ozbayoglu, A Murat and Unver, Hakki Ozgur. "Review of tool condition monitoring in machining and opportunities for deep learning." *The International Journal of Advanced Manufacturing Technology* Vol. 109 No. 3 (2020): pp. 953–974.

[20] Pimenov, Danil Yu, Bustillo, Andres, Wojciechowski, Szymon, Sharma, Vishal S., Gupta, Munish K. and Kuntoğlu, Mustafa. "Artificial intelligence systems for tool condition monitoring in machining: analysis and critical review." *Journal of Intelligent Manufacturing* (2022).

[21] Liu, Yuekai, Guo, Liang, Gao, Hongli, You, Zhichao, Ye, Yunguang and Zhang, Bin. "Machine vision based condition monitoring and fault diagnosis of machine tools using information from machined surface texture: A review." *Mechanical Systems and Signal Processing* Vol. 164 (2022): p. 108068.

[22] Yang, Yuhang and Shao, Chenhui. "Spatial interpolation for periodic surfaces in manufacturing using a Bessel additive variogram model." *Journal of Manufacturing Science and Engineering* Vol. 140 No. 6 (2018).

[23] Chen, Haotian, Yang, Yuhang and Shao, Chenhui. "Multi-task learning for data-efficient spatiotemporal modeling of tool surface progression in ultrasonic metal welding." *Journal of Manufacturing Systems* Vol. 58 (2021): pp. 306–315.

[24] Guo, Weihong (Grace), Jin, Jionghua (Judy) and Jack Hu, S. "Profile Monitoring and Fault Diagnosis Via Sensor Fusion for Ultrasonic Welding." *Journal of Manufacturing Science and Engineering* Vol. 141 No. 8 (2019).

[25] Nazir, Qasim and Shao, Chenhui. "Online tool condition monitoring for ultrasonic metal welding via sensor fusion and machine learning." *Journal of Manufacturing Processes* Vol. 62 (2021): pp. 806–816.

[26] Shi, Xinhua, Yu, Suiran, Li, Lin and Zhao, Jing. "Anvil state identification based on acceleration signals in ultrasonic metal welding of lithium batteries." *Journal of Manufacturing Processes* Vol. 70 (2021): pp. 67–77.

[27] Meng, Yuquan and Shao, Chenhui. "Physics-informed ensemble learning for online joint strength prediction in ultrasonic metal welding." *Mechanical Systems and Signal Processing* Vol. 181 (2022): p. 109473.

[28] Wu, Yulun, Meng, Yuquan and Shao, Chenhui. "End-to-end online quality prediction for ultrasonic metal welding using sensor fusion and deep learning." *Journal of Manufacturing Processes* Vol. 83 (2022): pp. 685–694.

[29] Zerehsaz, Yaser, Shao, Chenhui and Jin, Jionghua. "Tool wear monitoring in ultrasonic welding using high-order decomposition." *Journal of Intelligent Manufacturing* Vol. 30 No. 2 (2019): pp. 657–669.

[30] Yang, Yuhang, Dong, Zhiqiao, Meng, Yuquan and Shao, Chenhui. "Data-Driven Intelligent 3D Surface Measurement in Smart Manufacturing: Review and Outlook." *Machines* Vol. 9 No. 1 (2021): p. 13.

[31] Kurada, S. and Bradley, C. "A review of machine vision sensors for tool condition monitoring." *Computers in Industry* Vol. 34 No. 1 (1997): pp. 55–72.

[32] Dutta, S., Pal, S. K., Mukhopadhyay, S. and Sen, R. "Application of digital image processing in tool condition monitoring: A review." *CIRP Journal of Manufacturing Science and Technology* Vol. 6 No. 3 (2013): pp. 212–232.

[33] Lutz, Benjamin, Kisskalt, Dominik, Regulin, Daniel, Reisch, Raven, Schiffler, Andreas and Franke, Jörg. "Evaluation of Deep Learning for Semantic Image Segmentation in Tool Condition Monitoring." *2019 18th IEEE International Conference On Machine Learning And Applications (ICMLA)*: pp. 2008–2013. 2019.

[34] Wang, Haijun, He, Diqiu, Wu, Yunxin and Xu, Sheng. "Real-time welding condition monitoring by roughness information extracted from surface images." *Measurement* Vol. 191 (2022): p. 110833.

[35] Fisher, Ronald A. "The use of multiple measurements in taxonomic problems." *Annals of eugenics* Vol. 7 No. 2 (1936): pp. 179–188.

[36] Duda, Richard O, Hart, Peter E et al. *Pattern classification*. John Wiley & Sons (2006).